The International Journal of Advanced Manufacturing Technology (2020) 108:277–287
https://doi.org/10.1007/s00170-020-05370-2

ORIGINAL ARTICLE

Microhardness and residual stress of dissimilar and thick aluminum plates AA7181-T7651 and AA7475-T7351 using bobbin, top, bottom, and double-sided FSW methods

S. Delijaicov[1] · M. Rodrigues[1] · A. Farias[1] · M. D. Neves[1] · R. Bortolussi[1] · M. Miyazaki[2] · F. Brandão[2]

Received: 9 March 2020 / Accepted: 28 April 2020 / Published online: 12 May 2020

Abstract
Friction stir welding (FSW) is a relatively new manufacturing process (invented in 1991 at the Welding Institute, UK) and more than 5000 scientific articles have been published in the past 10 years in indexed journals demonstrating the robustness of the research. However, further research is necessary to ensure safe use of the technique for structural components, particularly with reference to the aeronautics industry. Residual stresses and their consequences on the life of welded products must be fully understood, in addition to their correlations with other properties such as hardness, strength, and microstructure. This paper is a part of the research being conducted to evaluate the impact of four FSW techniques (bobbin, top-sided, bottom-sided, and double-sided) on the mechanical properties in dissimilar thick joints (12.7 mm) of aluminum alloys (AA7181-T7651 and AA7475-T7351) used in the aeronautics industry. The residual stresses were measured using the incremental blind hole technique and analyzed using the integral method. The longitudinal residual stresses were all positive, with values between 100 and 200 MPa in the stir zone, whereas the transverse ones were all negative, with values between 0 and − 100 MPa. It was possible to verify that the Bobbin process produced lower values of residual stresses and demonstrated better stability in its distribution compared to all the other FSW methods tested.

Keywords AA7181-T7651 · AA7475-T7351 · FSW · Bobbin joint · Top-sided joint · Bottom-sided joint · Double-sided joint · Residual stress

1 Introduction

Friction stir welding (FSW), originally invented by Thomas et al. (1991), is a solid-state joining method adopted for joining aluminum alloys used in the aeronautics industry, including for dissimilar high-strength joints [1]. In this method, a rotating tool formed by a shoulder and pin is plunged into two plates and then translated to form the bead [2]. The forged force caused by the shoulder heats the metal and the rotate tool creates the flow and mixing of the materials, consolidating the weld. The thermal gradient resulting from the welding process, the compression state in the deformation zone, and the subsequent cooling of the joint contribute to the generation of a residual stress field and its characteristic microstructure [3]. Evaluation of residual stresses using the blind hole method of dissimilar double-sided, bobbin, top-sided, and bottom-sided FSW in thick plates of the AA7181-T7651 and AA7475-T7351 leveraged this project.

Conventional friction stir welding processes (top-sided and bottom-sided) require support plates in the tooling, which limits them to fewer complex configurations. Consequently, defects such as a lack of penetration, porosity, and cavities can be generated. To homogenize the process with improved material flow [4], the double-sided and bobbin processes were proposed while avoiding the defects and stabilizing the profiles of hardness and residual stresses along the thickness of the plates. The first process entails two welding passes, one on each side of the plates, whereas the other requires a single pass with a two-shoulder tool [5]. The bobbin process is suitable for closed structures such as pipes or hollow extrusions.

Xu and Liu (2015) demonstrated that the double-sided FSW process leads to substantial grain refinement of

✉ S. Delijaicov
sergiode@fei.edu.br

[1] University Center of FEI, São Bernardo do Campo, Brazil

[2] EMBRAER, São José dos Campos, Brazil

Table 1 Chemical compositions

Element weight	Zn	Mg	Cr	Mn	Cu	Si	Fe	Ti	Zr
AA7181	5.20–6.20	1.90–2.60	0.18–0.25	0.06	1.20–1.90	0.10	0.12	0.06	–
AA7475	6.70–7.90	1.70–2.20	0.04	0.15	1.20–1.90	0.08	0.10	0.06	0.08–0.18

AA7085-T7452 Al alloy, with grain sizes less than 2 μm, improving the strength and generating residual stress owing to the high plastic work [6]. However, Goebel, J. et al. (2017) studied the bobbin FSW process with AA2198-T851 alloy [7]. They observed that the stirred zone experienced the highest shear rates and peak temperatures and the fully recrystallized zone had fine grains with an average grain diameter of 6 μm and improved mechanical properties. Xu et al. (2018) compared the local and global mechanical properties of the bobbin tool and the conventional friction stir-welded AA7085-T7452 aluminum thick plate [8]. The results indicated that the microhardness distribution of both FSW joints resembled a "W" shape, and the lowest hardness was located in the heat-affected zone on the advancing side. Cetkin et al. (2019), when studying the microstructure and mechanical properties of AA7075 and AA5182 jointed by FSW, show that microhardness is affected by pin geometry and welding parameters and that hardness values differed with the influence of heat [9]. The minimum hardness values were obtained for the rotation speed of 980 rpm and feed rate of 108 mm/rev while the maximum hardness values for the rotation speed of 1325 rpm and feed rate of 108 mm/rev. The minimum and maximum hardness values were 67.1 and 87 HV, respectively. According to [10] when researching the friction stir welds of dissimilar AA2XXX/AA7XX alloys, regions whose hardness were less than 110 HV 0.05 are located on the AA7020 side HAZ for all conditions. The origin of this weak zone was mainly linked to precipitates that worsened in the base metal due to exposure to temperatures in the range of 225 to 260 °C. Exposure time to this critical temperature range may also play a role in controlling the hardness. Jimenez-Mena et al. (2019) studying the main origin of longitudinal residual stresses in the aluminum showed the deformation caused by non-uniform thermal field and phase transformation [11]. During the cooling, the nugget tends to shrink. However, the shrinkage is constrained by the surroundings that remained at lower temperature. Tensile residual stresses thus appear in the stir and thermo-mechanically affected zones while the surrounding regions experience compressive residual stresses. Yu et al. (2018) studying the welding stress induced by friction stir welding, showed that a higher tensile stress appears below the tool shoulder with increasing rotation speed [12]. Higher feed speed introduces lower tensile stress on the welded

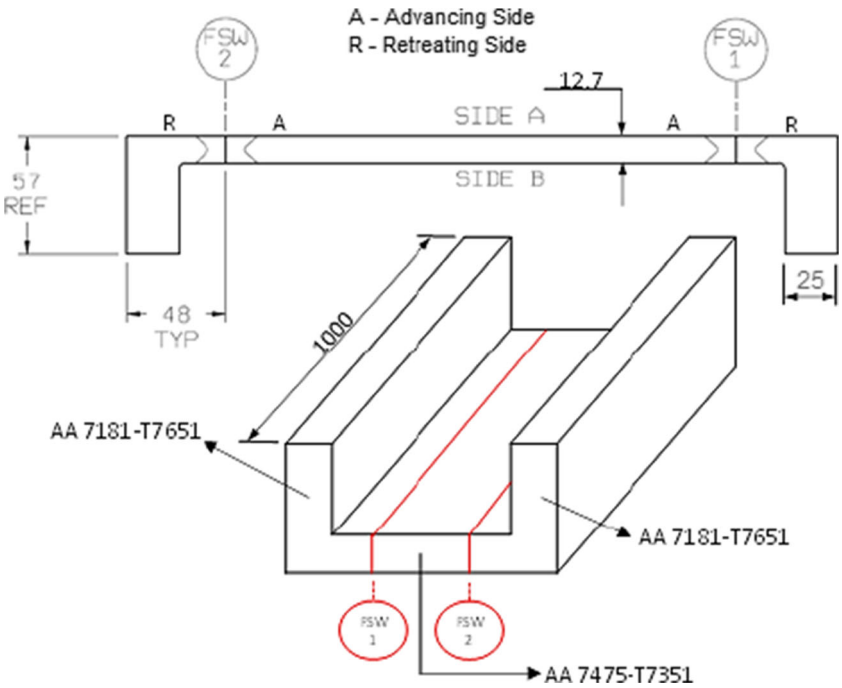

Fig. 1 Basic shape of machined aircraft spars

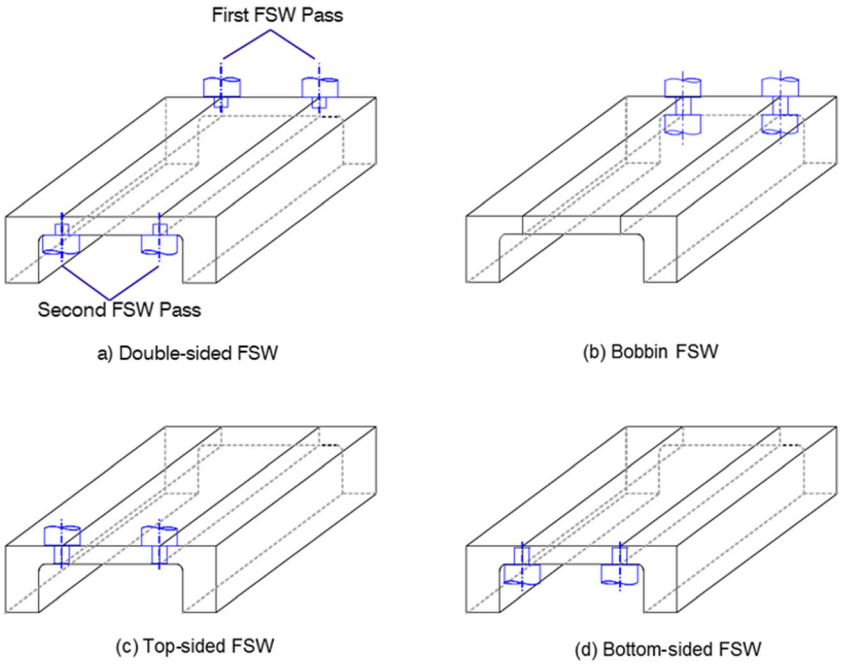

Fig. 2 FSW process modalities

Table 2 FSW parameters

	ω (rpm)	v (mm/min)	F (kN)	Tilt angle (°)	ω/v (rev/mm)
Top- and bottom-sided	300	250	80	2	1.2
Double-sided	300	350	80	2	0.86
Bobbin	90	90	–	–	1

structure and there is tensile stress in the heat-affected zone and compression stress in the elastic zone. Papan et al. (2014) performed ultrasonic measurements of residual stresses caused by severe thermomechanical deformation during FSW of AA7075-T6 plates and obtained "M"-shaped longitudinal stresses measuring between 180 and 230 MPa in the nugget, and transverse stresses in the range of 35 and 55 MPa [13]. Ji et al. (2015) conducted research on FSW of a 12.3-mm-thick AA7075-T651 plate at a welding speed of 100 mm/min and a rotating speed of 400 rpm parallel to the rolling direction [14]. Using X-ray and neutron diffractions techniques, they obtained maximum stress of approximately 150 MPa with similarity in profiles. Aval (2015) studied the impact of welding heat input and post-weld natural aging on the residual stress of dissimilar FSW of AA6082-T6 and AA7075-T6 thick plates and obtained values of 120 MPa using the XRD technique with Cr Kα radiation, with the X-ray tube

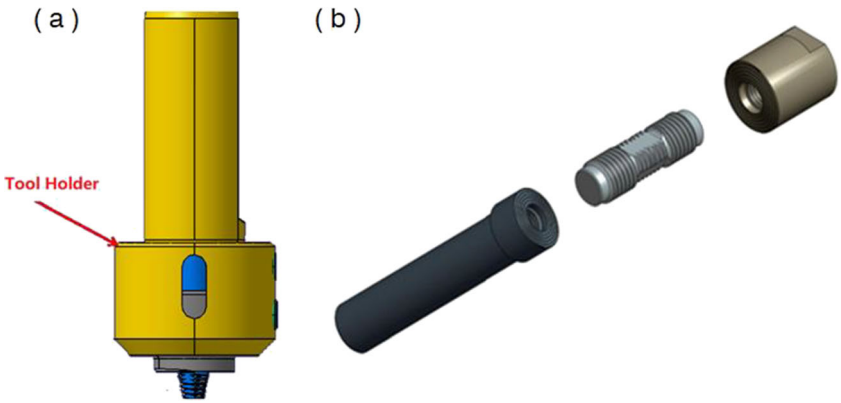

Fig. 3 FSW tools: **a** triflat probe for top-sided, bottom-sided, and double-sided FSW, **b** flat cylindrical outer surface for bobbin FSW

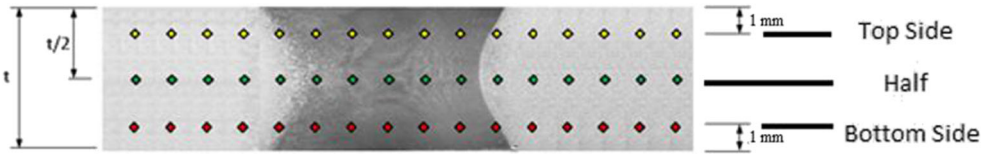

Fig. 4 Three lines of hardness measurements

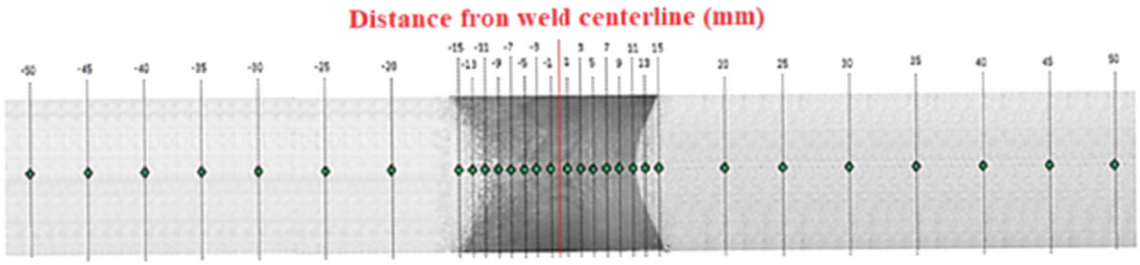

Fig. 5 Hardness measurement positions

operating at 20 kV at a target current of 4 mA [15]. Haghshenas et al. (2017) evaluated the distribution of residual stress in FSW joints in the AA7075 alloy using a semi-destructive technique (depth-controlled nanoindentation) and obtained maximum values of approximately 220 MPa [16].

The objective of this study is to evaluate the differences in behavior experimentally (in terms of the microhardness and residual stresses) resulting from the FSW process in thick and dissimilar aluminum plates AA7181-T7651 and AA7475-T7351 when welded using the bobbin, double-, top-, and bottom-sided FSW techniques.

2 Materials and methods

The aluminum alloys AA7181-T7651 and AA7475-T7351 used for FSW tests are considered strategically

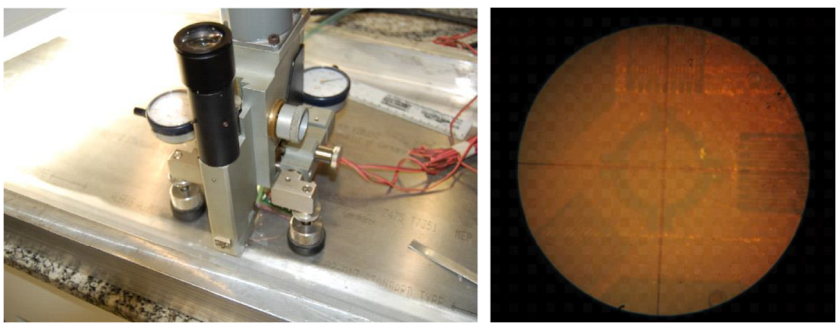

Fig. 6 Drilling equipment

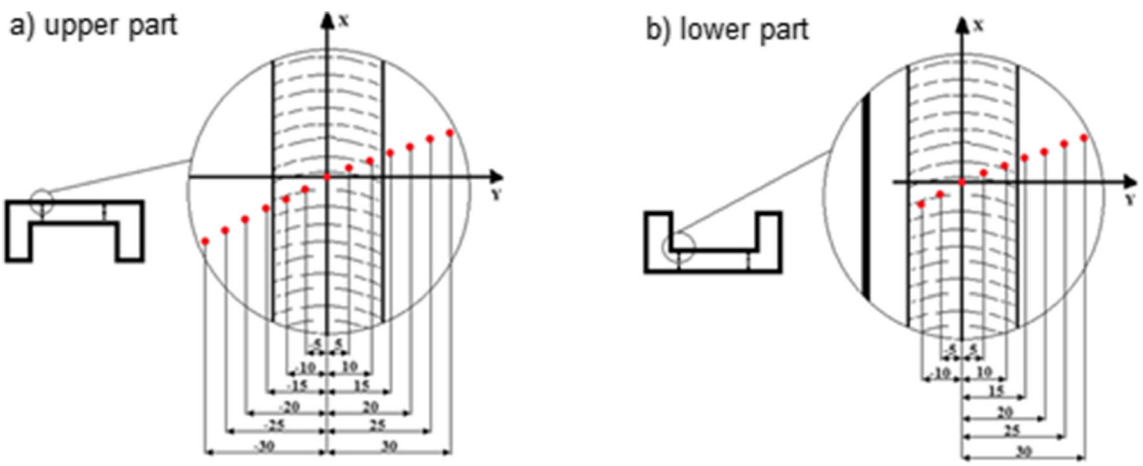

Fig. 7 Points of residual stress measurement

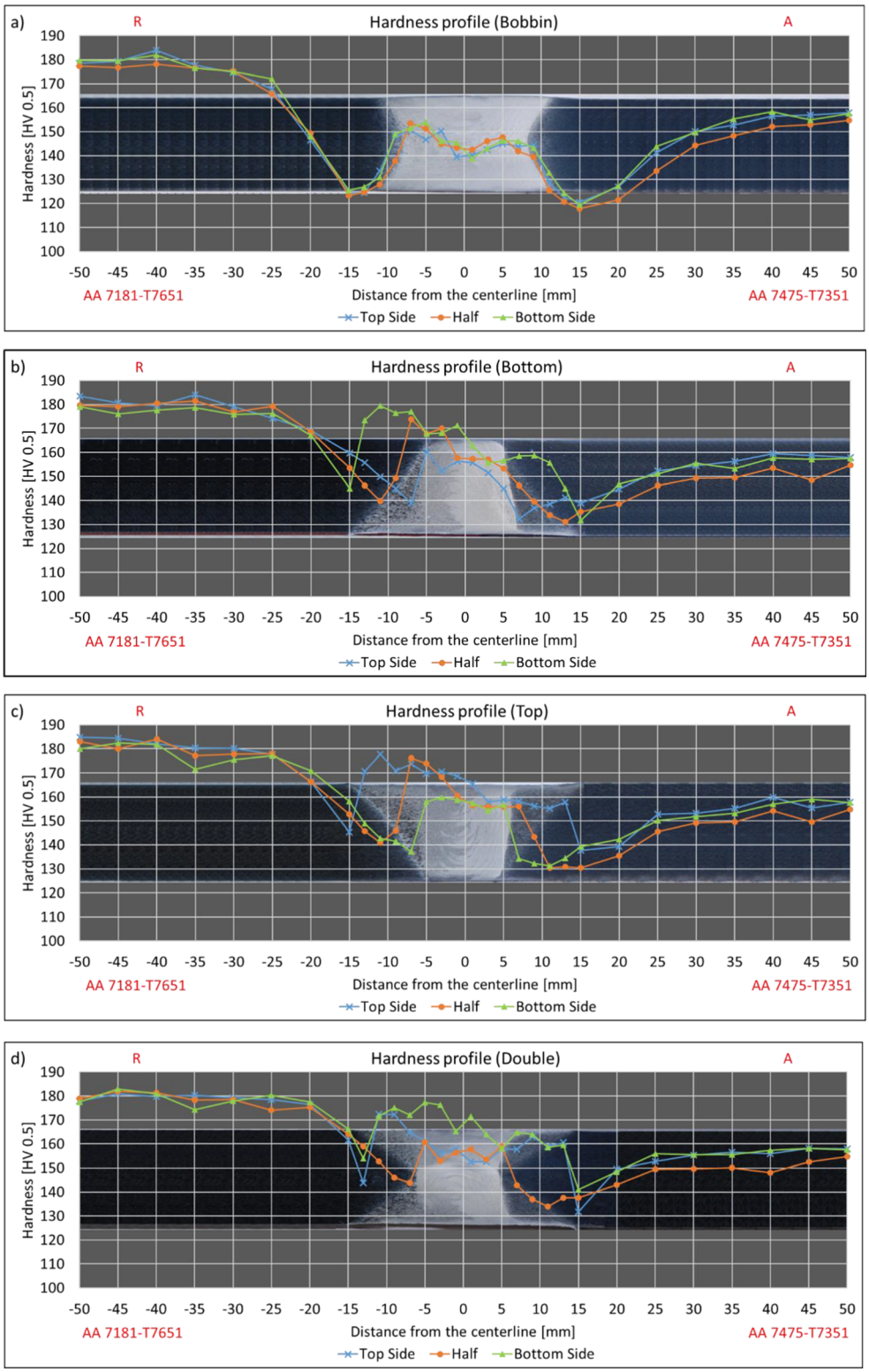

Fig. 8 Hardness profile modalities: **a** bobbin, **b** bottom-sided, **c** top-sided, **d** double-sided

significant for the aerospace industry. They demonstrate significant mechanical resistance owing to their respective chemical compositions and when subjected to heat treatment. The details of the chemical compositions are provided in Table 1.

Four test specimens were welded using FSW in four process modalities: double-sided, bobbin, top-sided, and bottom-sided, as illustrated in Figs. 1 and 2. To form the C profile, two other L profiles (AA7181-T7651) were welded to the 12.7-mm-thick center plate

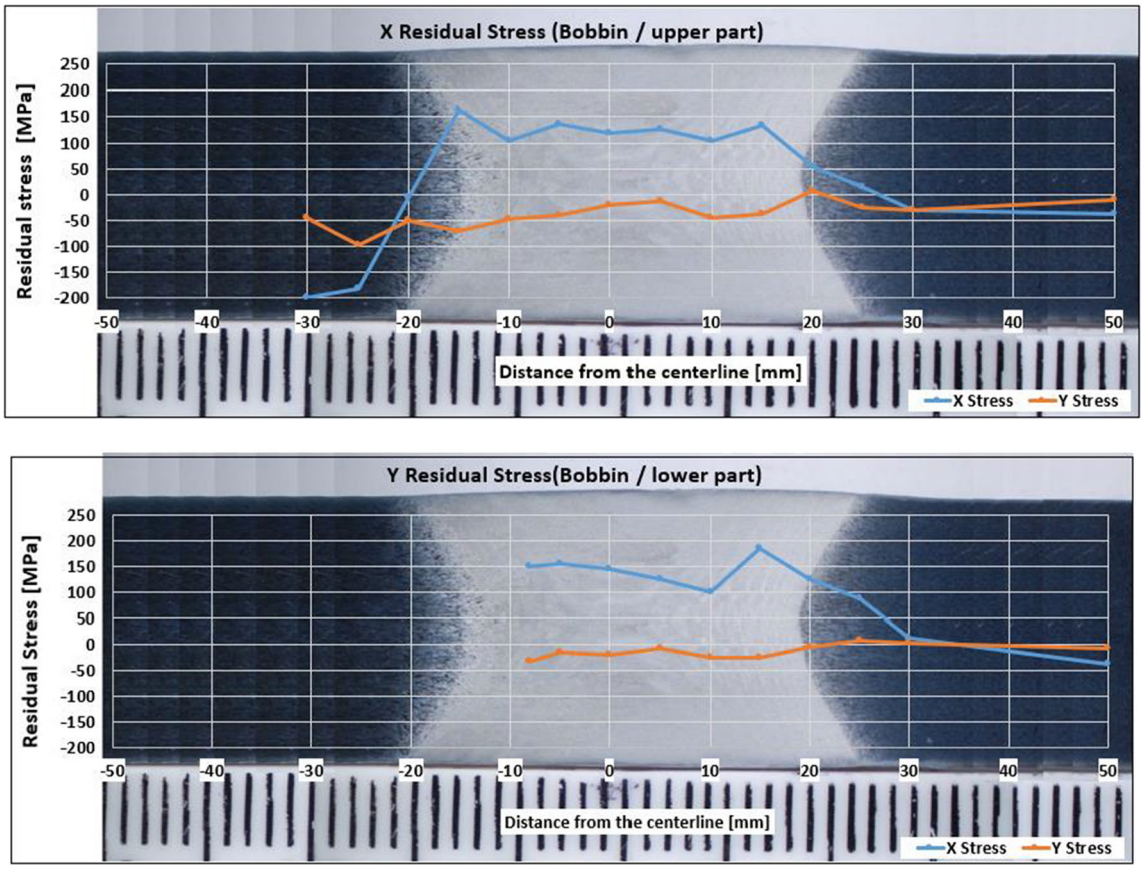

Fig. 9 Bobbin residual stress profile: longitudinal direction (*X*), transverse direction (*Y*)

(AA7475-T7351) to simulate the basic shape of machined aircraft spars.

The welding parameters were chosen after preliminary planning to ensure the best performance of the process in terms of the finish of the joint and welding efficiency. The independent variables were defined as rotational speed in rpm, tool travel speed in mm/min, and tool tilt angle in degrees, as listed in Table 2.

The joints were produced at the TWI Welding Institute. For the top-sided, bottom-sided, and double-sided FSW, the equipment used to join the specimens was the SuperStir machine, and the PowerStir machine was used for bobbin FSW. The tools used for top-sided, bottom-sided, and double-sided FSW were the conical triflat threaded probe with scrolled shoulders and triflat threaded probe with scrolled shoulders for bobbin FSW (Fig. 3).

The specimens used for metallographic examination were prepared by cutting the welded joints and polishing with different grades of emery sheets followed by polishing with diamond paste. The metallographic analyses were performed by light microscopy after etching with the Keller reagent (10 ml of hydrofluoric acid, 15 ml of concentrated hydrochloric acid, 25 ml of concentrated nitric acid, and 50 ml of distilled water).

The microhardness indentation was conducted with a Shimadzu microhardness meter model HMV-2. The Vickers microhardness test was used with a load of 4.903 N. Microhardness was measured on an Olympus BX60M microscope coupled with an Olympus SC30 camera. For measuring and calculating the microhardness, AnalySIS software version 5.1 from Olympus Soft Imaging Solutions GmbH was used.

The measurement strategy is illustrated in Figs. 4 and 5, i.e., three lines of measurements in the cross-sections of the specimens from − 50 to + 50 mm in relation to the centerline.

The residual stresses were measured using the blind hole technique with SINT-MTS3000 equipment (Fig. 6). Milling cutters with a tapered milling top 1.8 mm in diameter were used along with Vishay rosettes CEA-13-062UL-120.

For the residual stress measurements, 13 holes were drilled in the upper part of the plates, as illustrated in Figs. 7a, and 8, holes were drilled in the lower part (the number of holes was less because of space limitation for the measurements), as illustrated in Fig. 7b. At each measurement point, the residual stress profile was generated up to a depth of 0.8 mm. The 0.2-mm-layer measurement was removed to avoid erroneous calculations because of the burrs generated by the welding process.

The data were collected using the software Residual Stress Measurement System RESTAN version 5.3.1 and treated in the software Hdrill version 3.01 using the integral method to calculate the welding line stresses.

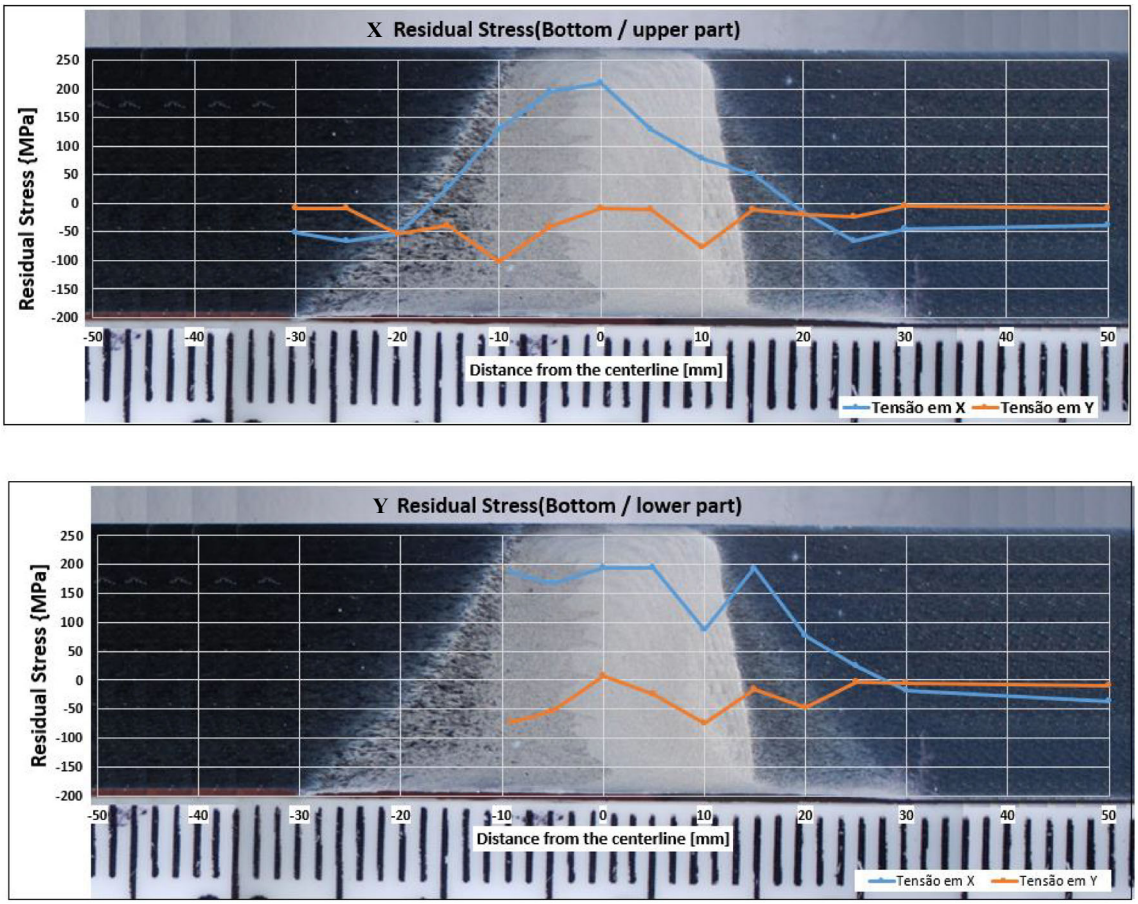

Fig. 10 Bottom-sided residual stress profile: longitudinal direction (X), transverse direction (Y)

3 Results and discussion

3.1 Hardness measurement

For the base materials of the alloys AA7181-T7651 and AA7475-T7351, hardness values of 180 and 150 HV, respectively, were measured. The distribution of hardness in the FSW joints obtained using the four welding techniques are plotted in Fig. 8. Although the geometry/dimension of the welding tool also affects the microhardness profile, Fig. 9a indicates that the bobbin process leads to significant stability in the distribution of hardness. This can be explained by the more uniform action of the thermal input because of the upper and lower shoulders of the tool acting simultaneously on the plates. It was observed that the hardness profiles across the joint configurations of bottom-sided, top-sided, and double-sided FSW are similar in shape and values (Fig. 8b–d).

The hardness and distribution are subjected to the thermal and mechanical conditions that the material experiences during the FSW process. Therefore, the hardness varies from zone to zone as well as point to point within the zones. The hardness profiles depend mainly on the precipitate distributions in the weld [17]. Regions outside the weld nugget usually have precipitate distributions that strongly depend on the exposure to the potentially different thermal histories.

It is observed that in the affected zones of all joints, Fig. 9a–d, hardness tends to increase near the base metals. The lowest mean hardness in the HAZ (heat-affected zone) region was observed in the bobbin method (Fig. 8a) owing to the efficient thermal input of this method. At the bottom- and top-sided joints (Fig. 8b and c), higher hardness are observed at the tool shoulder sides because of the larger areas of contact with the materials, resulting in higher friction, as observed by [18]. The underside hardness of the joint was observed on the double side (Fig. 8d) because this was the final processed side. In all processes, Fig. 8a–d, the hardness in the nugget region was lower than that at the base materials owing to the dissolution of resistant precipitates during the thermal cycles of the welds, as observed by [19]. This is also the reason for the "W" shape of the distribution, as reported by [7].

3.2 Residual stresses

Figures 9, 10, 11, and 12 present the residual stress distributions of the four welding techniques in the longitudinal and transversal directions (directions *X* and *Y*)

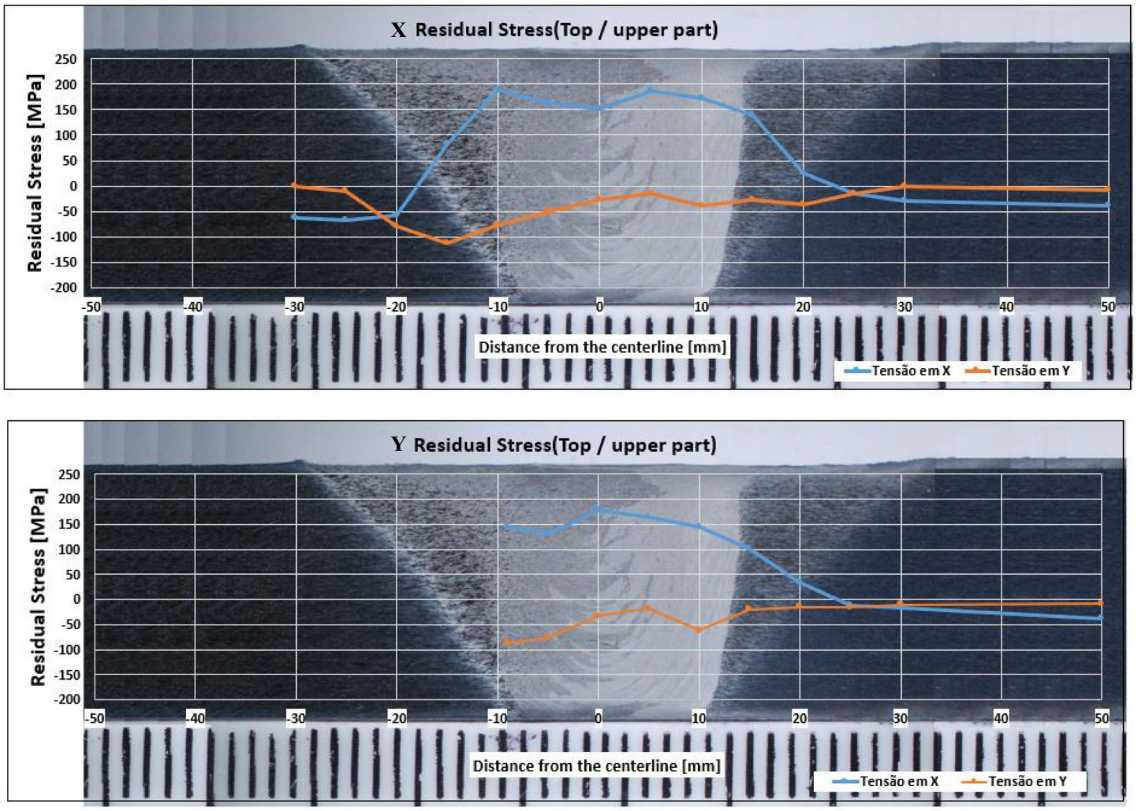

Fig. 11 Top-sided residual stress profile: longitudinal direction (*X*), transverse direction (*Y*)

on the top and bottom surfaces of the joints, respectively. The measurements along the transverse direction (direction *Y*) of the joints were restricted to − 10 mm from the centerline because of the limit imposed by the fixture device.

In the base materials, the residual stresses are compressive (approximately 50 MPa), owing to the lamination process of the plates. The stirring of the plasticized material in the deformation zone and the thermal gradient from the nugget zone to the base material are the factors that generate the residual stresses.

It should be noted that the residual stresses are all tractive (positive) in the longitudinal directions and compressive (negative) in the transverse directions. Residual stresses generated by the bobbin method are less tractive than the others owing to the higher thermal input during the welding process. Generally, an increase in the welding heat results in a contracted residual stress and extended tensile stress region, as observed by [15].

The profiles had an "M" shape, and the maximum tensile residual stresses were located near the edge of the tool shoulder. It was observed in all profiles that the maximum stress values were in the retreating side of the most resistant alloy, as found by [20]. An inverse correlation was observed between the hardness and residual stress.

3.3 Macroscopic and microscopic observations

Macroscopic observations carried out in the cross-section of the welded joints performed under various conditions indicated the formation of similar regions. The regions denominated by the stir zone (SZ), thermo-mechanically affected zone (TMAZ), and heat-affected zone (HAZ) were observed in all joints. However, the macrographs are different based on the shape of the welding. The welding parameters, heat input, and position of the tool all affect the distribution of heat in the joint. Figure 13 presents the optical micrographs of the SZ, TMAZ, and HAZ for all the FSW techniques.

The heat-affected zone is created when the base metal is subjected to a thermal cycle and, therefore, the original microstructure is modified, although the characteristic and elongated grains of the mechanically formed base metal still exist. The HAZ presented in Fig. 14 indicates relatively thinner grain than the base metal.

In the TMAZ region, the FSW process deforms the material structure (Fig. 15). The temperature reached during welding is not enough to cause dynamic recrystallization. However, the heat from the adjacent side zone results in larger grain size compared to that in the SZ.

The stir zone observed in Fig. 15 consists of fine equiaxial grains, which can be attributed to dynamic recrystallization.

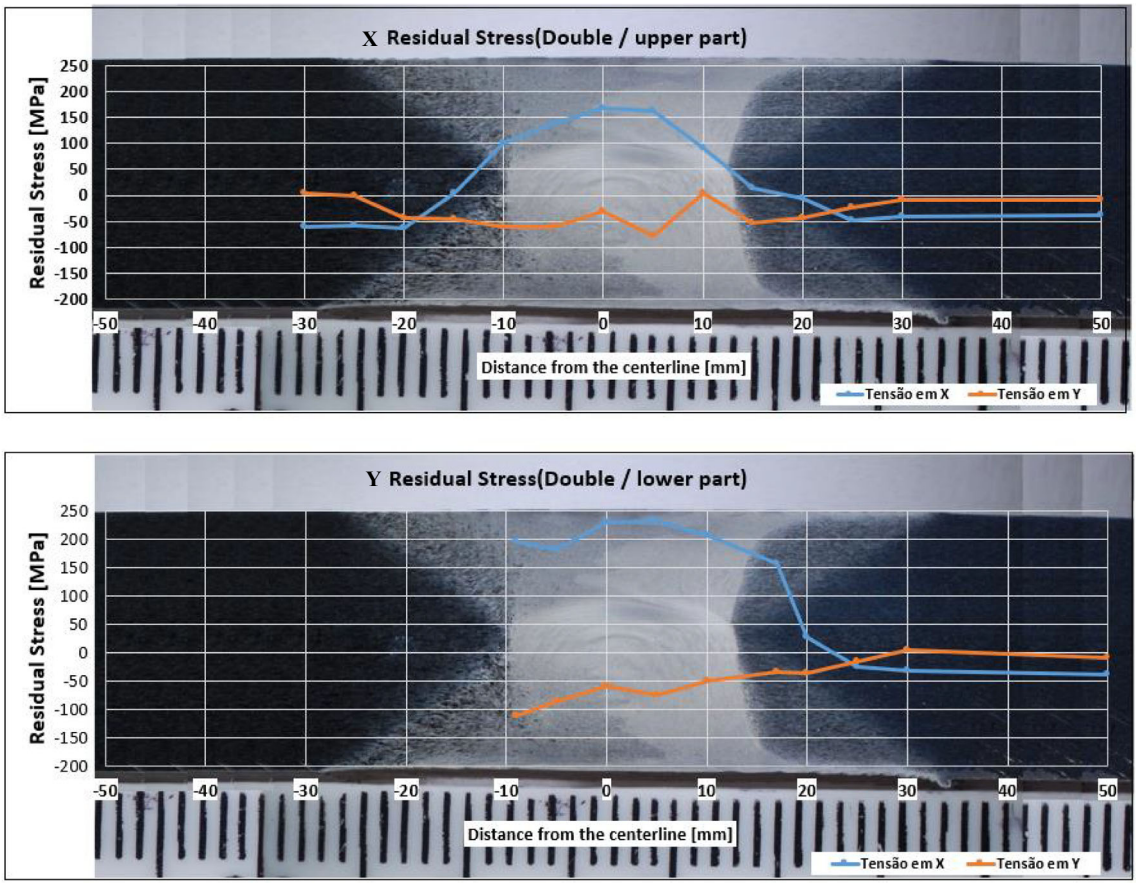

Fig. 12 Double-sided residual stress profile: longitudinal direction (*X*), transverse direction (*Y*)

Clear evidence of plastic deformation is observed in this region. A common observation of the SZ in FSW is the appearance of a series of circular or elliptical features in metallographic sections, often referred to as onion rings.

Grain growth occurs simultaneously as the temperature increases and low-angle sub-grains begin to form through a dynamic recovery process, as presented in Fig. 16. Continuous dynamic recrystallization occurs when dislocations are continuously introduced into the sub-grains by further deformation. The growth and rotation of the sub-grains occur while accommodating more dislocations at their limits, forming equiaxial recrystallized grains with high-angle grain contours. Plastic deformation

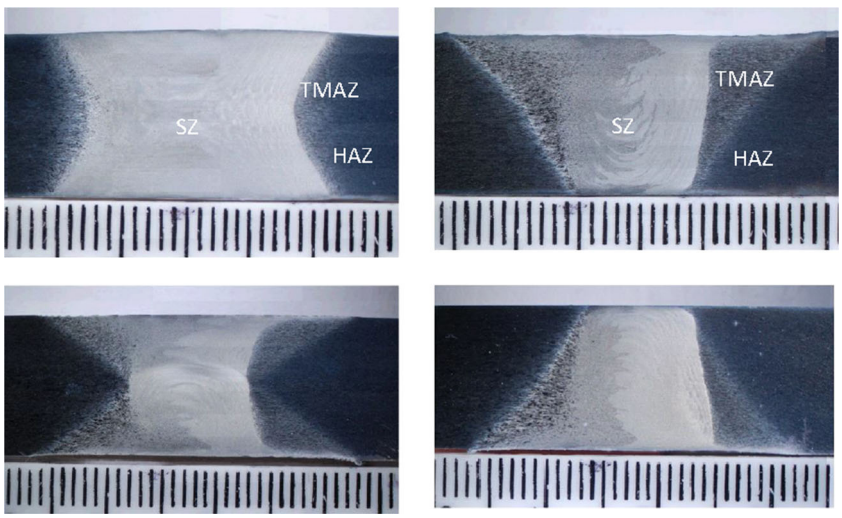

Fig. 13 Optical micrographs of SZ, TMAZ, and HAZ for all FSW techniques (scale in millimeters)

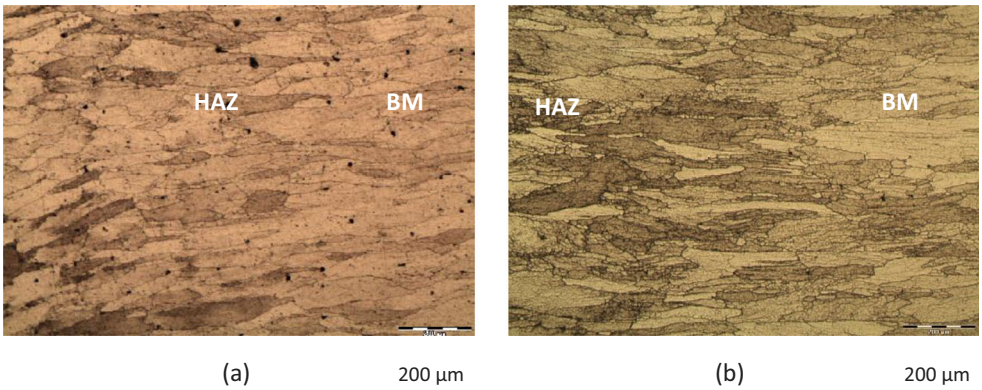

Fig. 14 Images obtained through optical microscopy: **a** AA7475-T7351A and **b** AA7181-T7651

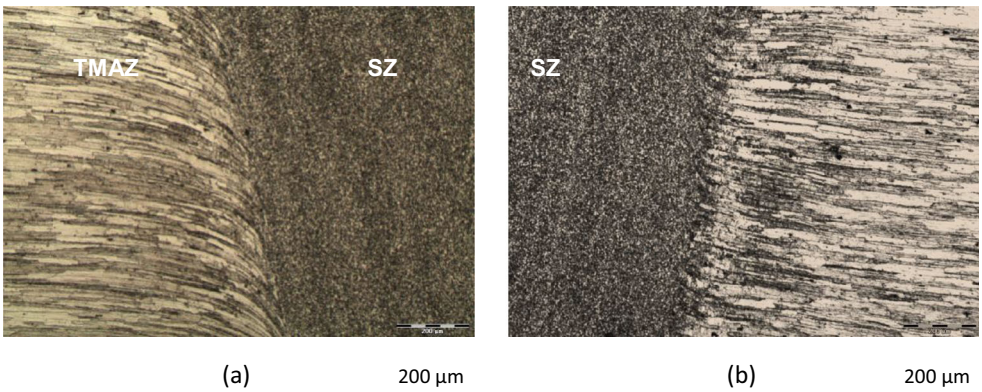

Fig. 15 Images obtained through optical microscopy: **a** AA7475-T7351A and **b** AA7181-T7651

continues with the repeated introduction of dislocations, and the process continues until the end of the thermomechanical cycle, which occurs with partial recovery.

4 Conclusions

This study was performed to evaluate experimentally the behavioral differences, in terms of microhardness and residual stresses, resulting from the FSW process in thick and dissimilar aluminum plates AA7181-T7651 and AA7475-T7351 when welded using the bobbin, double-, top-, and bottom-sided FSW techniques. The main conclusions were as follows:

- The bobbin modality proved to be the most suitable among the four techniques for welding thick plates using FSW while considering only residual stress.
- The longitudinal residual stresses were all positive, with values between 100 and 200 MPa in the stir zone, whereas the transverse ones were all negative, with values between 0 and − 100 MPa.
- It was possible to verify that the bobbin process produced lower values of residual stresses.

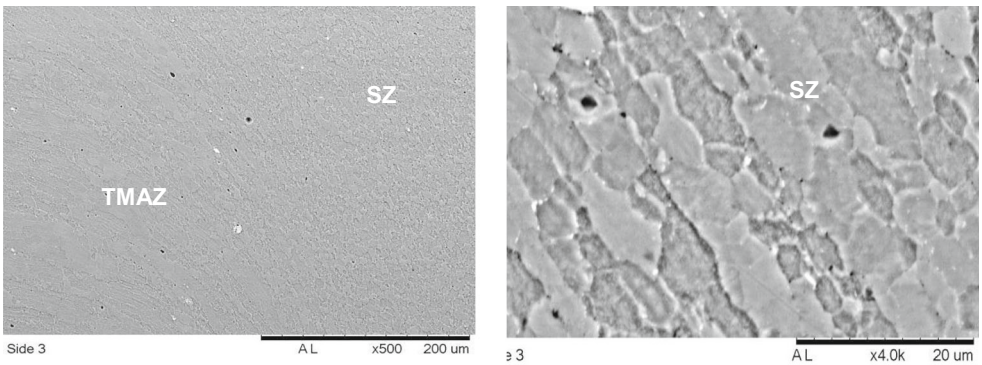

Fig. 16 Images obtained using scanning electronic microscopy: **a** interface AA7475-T7351A, **b** sub-grains in SZ

- The bobbin process demonstrated improved stability in its residual stress distribution, which could also be observed in the distribution of microhardness.

Compliance with ethical standards

Conflict of interest The authors declare that they have no conflict of interest.

References

1. Thomas WM, Nicholas ED, Needham JC, Murch MG, Temple-Smith P, Dawes CJ (1991) Improvements relating to friction welding. GB patent no:9125978–9125978
2. Wu H, Chen Y, Strong D, Prangnell P (2015) Stationary shoulder FSW for joining high strength aluminum alloys. J Mater Process Technol 221:187–196
3. Padhy GK, Wu CS, Gao S (2017) Friction stir based welding and processing technologies - processes, parameters, microstructures and applications: a review. J Mater Sci Technol 14:1–38
4. Wang FF, Li WY, Shen J, Wen Q, Santos JF (2018) Improving weld formability by a novel dual-rotation bobbin tool friction stir welding. J Mater Sci Technol 34:135–139
5. Esmaily M, Mortazavi N, Osikowicz W, Hindsefelt H, Svensson JE, Halvarsson M, Martin J, Johansson LG (2016) Bobbin and conventional friction stir welding of thick extruded AA6005-T6 profiles. Mater Des 108:114–125
6. Xu W, Liu J (2015) Microstructure evolution along thickness in double-side friction stir welded 7085 Al alloy. Trans Nonferrous Metals Soc China 25:3212–3222
7. Goebel J, Reimann M, Norman A, Santos FF (2017) Semi-stationary shoulder bobbin tool friction stir welding of AA2198-T851. J Mater Process Technol 245:37–45
8. Xu W, Luo Y, Zhang W, Fu MW (2018) Comparative study on local and global mechanical properties of bobbin tool and conventional friction stir welded 7085-T7452 aluminum thick plate. J Mater Sci Technol 34:173–184
9. Cetkin E, Çelik YH, Temiz S (2019) Microstructure and mechanical properties of AA7075/AA5182 jointed by FSW. J Mater Process Technol 268:107–116
10. Bertrand R, Robe H, Texier D, Zedan Y, Feulvarch E, Bocher P (2019) Analysis of AA2XXX/AA7XXX friction stir welds. J Mater Process Technol 271:312–324
11. Jimenez-Mena N, Sapanathan T, Drezet JM, Pirling T, Jacques PJ, Simar A (2019) Residual stresses of friction melt bonded aluminum/steel joints determined by neutron diffraction. J Mater Process Technol 266:651–661
12. Yu H, Zheng B, Lai X (2018) A modeling study of welding stress induced by friction stir welding. J Mater Process Technol 254:213–220
13. Papan H, Bahemmat P, Haghpanahi M, Valipour A (2014) Ultrasonic measurements of residual stresses caused by severe thermomechanical deformation during FSW. Exp Mech 54:1587–1596
14. Ji P, Yang Z, Zhang L, Ji V, Klosek V (2015) Residual stress distribution and microstructure in the friction stir weld of 7075 aluminum alloy. J Mater Sci 50:7262–7270
15. Aval HJ (2015) Microstructure and residual stress distributions in friction stir welding of dissimilar aluminum alloys. Mater Des 87:405–413
16. Haghshenas M, Gharghouri MA, Bhakhri V, Klassen RJ, Gerlich AP (2017) Assessing residual stresses in friction stir welding: neutron diffraction and nanoindentation methods. Int J Adv Manuf Technol 93:3733–3747
17. Cabibbo M, Forcellese A, Mehtedi E, Simoncini M (2014) Double side friction stir welding of AA6082 sheets: microstructure and nanoindentation characterization. Mater Sci Eng A 590:209–217
18. Sahu PK, Pal S (2017) Mechanical properties of dissimilar thickness aluminum alloy weld by single/double pass FSW. J Mater Process Technol 243:442–455
19. Ahmeda MMZ, Ataya S, Seleman MMS, Ammar HR, Ahmed E (2017) Friction stir welding of similar and dissimilar AA7075 and AA5083. J Mater Process Technol 242:77–91
20. Zapata J, Toro M, López D (2016) Residual stresses in friction stir dissimilar welding of aluminum alloys. J Mater Process Technol 229:121–127